Oncogene (2003) 22, 8912–8923

www.nature.com/onc

Segregation of NF-κB activation through NEMO/IKKγ by Tax and TNFα: implications for stimulus-specific interruption of oncogenic signaling

Hidekatsu Iha[1], Karen V Kibler[1], Venkat RK Yedavalli[1], Jean-Marie Peloponese[1], Kerstin Haller[1], Akiko Miyazato[1], Takefumi Kasai[1] and Kuan-Teh Jeang*[,1]

[1]*Laboratory of Molecular Microbiology, Molecular Virology Section, National Institute of Allergy and Infectious Diseases, National Institutes of Health, Bethesda, MD 20892-0460, USA*

Nuclear factor-κB essential modulator (NEMO), also called IKKγ, has been proposed as a 'universal' adaptor of the I-κB kinase (IKK) complex for stimuli such as proinflammatory cytokines, microbes, and the HTLV-I Tax oncoprotein. Currently, it remains unclear whether the many signals that activate NF-κB through NEMO converge identically or differently. We have adopted two approaches to answer this question. First, we generated and targeted intracellularly three NEMO-specific monoclonal antibodies (mAbs). These mAbs produced two distinct intracellular NF-κB inhibition profiles segregating TNFα from Tax activation. Second, using NEMO knockout mouse fibroblasts and 10 NEMO mutants, we found that different regions function *in trans* either to complement or to inhibit dominantly TNFα, IL-1β, or Tax activation of NF-κB. For instance, NEMO (1—245 amino acids) supported Tax-mediated NF-κB activation, but did not serve TNFα- or IL-1β signaling. Altogether, our findings indicate that while NEMO 'universally' adapts numerous NF-κB activators, it may do so through separable domains. We provide the first evidence that selective targeting of NEMO can abrogate oncogenic Tax signaling without affecting signals used for normal cellular metabolism.
Oncogene (2003) **22,** 8912–8923. doi:10.1038/sj.onc.1207058

Keywords: Tax; HTLV-I; adult T-cell leukemia; NEMO/IKKγ; TNFα; NF-κB; oncogenic transformation

Introduction

The nuclear factor-κB (NF-κB) family of eucaryotic transcription factors plays multiple roles in the inducible expression of genes involved in diverse biological processes, including development, immune/inflammatory responses, cell growth/death, stress responses, and carcinogenesis. NF-κB is activated in response to physical and chemical stress, bacterial lipopolysaccharide, double-stranded RNA, T- and B-cell mitogens, and proinflammatory cytokines (Rothwarf and Karin, 1999; Beyaert *et al*., 2000; Karin and Lin, 2002; Li and Verma, 2002), among others. In resting cells, the majority of NF-κB is sequestered in the cytoplasm in complexes with I-κB inhibitory proteins. Phosphorylation of I-κBs leads to protein-ubiquitination that is followed by proteosome-mediated degradation. Once freed from I-κB, NF-κB translocates into the nucleus and activates the transcription of cognate genes (Chen *et al*., 1996; Whiteside and Israel, 1997). Recent findings show that the I-κB kinase (IKK) complex that is composed of at least three subunits, catalytic IKKα and IKKβ, and regulatory NF-κB essential modulator (NEMO), critically phosphorylates I-κB proteins (Scheidereit, 1998; Karin, 1999; Courtois *et al*., 2001).

IKKα and IKKβ are highly homologous proteins with an N-terminal protein kinase domain as well as leucine zipper and helix–loop–helix motifs (DiDonato *et al*., 1997; Mercurio *et al*., 1997; Zandi *et al*., 1997). Despite their structural similarities, IKKα and IKKβ have distinct functions. IKKβ is approximately 20-fold more active than IKKα in phosphorylating I-κB (Mercurio *et al*., 1997); and IKKβ, but not IKKα, knockout mouse fibroblasts have impaired NF-κB activation in response to proinflammatory cytokines (Hu *et al*., 1999; Li *et al*., 1999a, b, d; Takeda *et al*., 1999; Tanaka *et al*., 1999). The NEMO (IKKγ) subunit of the IKK complex is a coiled-coil protein devoid of kinase activity (Rothwarf *et al*., 1998; Yamaoka *et al*., 1998). However, genetic experiments have shown that loss of NEMO function entirely eliminates NF-κB activation by all proinflammatory cytokines (Makris *et al*., 2000; Rudolph *et al*., 2000; Schmidt-Supprian *et al*., 2000). Current thinking is that NEMO functions as a 'universal' scaffold protein adapting various upstream NF-κB-activating signals (Courtois *et al*., 1997) to a high molecular weight (HMW) intracellular IKKα/β complex (DiDonato *et al*., 1997; Mercurio *et al*., 1997; Zandi *et al*., 1997). However, in its role as a 'universal' adaptor, how NEMO integrates the various activating signals, and whether all impinges on NEMO identically or divergently remain unclear. If divergent mechanisms are utilized, conceivably one could selectively attenuate

*Correspondence: K-T Jeang, Building 4, Room 306, 9000 Rockville Pike, Bethesda, MD 20892-0460, USA; E-mail: kj7e@nih.gov
Received 15 May 2003; revised 28 July 2003; accepted 31 July 2003

some NF-κB stimuli without affecting others. Should one have enough information regarding separable NEMO functional domains, conceivably selective intracellular disruption could be effected using small-cell-permeable peptides (May *et al*., 2000).

NF-κB plays parallel roles in immunity/inflammation, apoptosis, and cellular proliferation (Karin *et al*., 2002). In selective settings, interdiction against one NF-κB activity might be highly useful provided that the other NF-κB axes are preserved. For example, in treatment approaches for adult T-cell leukemia (ATL), an HTLV-I-engendered leukemia (Hinuma *et al*., 1981; Yoshida *et al*., 1982; Yoshida, 2001), selective abrogation of Tax-NF-κB signaling without affecting other paths used for immunity or for protecting normal cells from TNFα-induced killing would be very desirable. Such an interruption could be possible if NEMO structure/function can be dissected in a manner that segregates Tax from proinflammatory cytokine activation. Here, we show molecularly discrete signaling through NEMO by Tax and TNFα. We provide evidence that activation by the former can be selectively abrogated without affecting the latter.

Results

NEMO-specific monoclonal antibodies differentially inhibit intracellular Tax versus TNFα signaling

Monoclonal antibodies (mAbs) directed to human extracellular receptors/proteins have achieved emerging therapeutic promise (Ranson and Sliwkowski, 2002; Ghosh *et al*., 2003). With the advent of efficient protein-transfection technology, targeting and/or characterization of intracellular factors using mAbs seems increasingly feasible. To better understand the nuances of NEMO modulation, we generated four new anti-NEMO IgG1 mAbs, AB6-9, FG10-3, DA10-12, and EA2-6, by immunizing Balb/C mice with full-length human NEMO. Recognition specificities were characterized by probing nine immunoblotted GST-NEMO subfragments (Figure 1a, b). Thus, two monoclonals, FG10-3 (Figure 1b, panel 1) and DA10-12 (Figure 1b, panel 2), strongly recognized NEMO N-terminal amino acids 1–137. However, FG10-3 and DA10-12 appear to be distinct, based on their slightly different affinities for fragments 61–137 and 61–262 (Figure 1b, panels 1 and

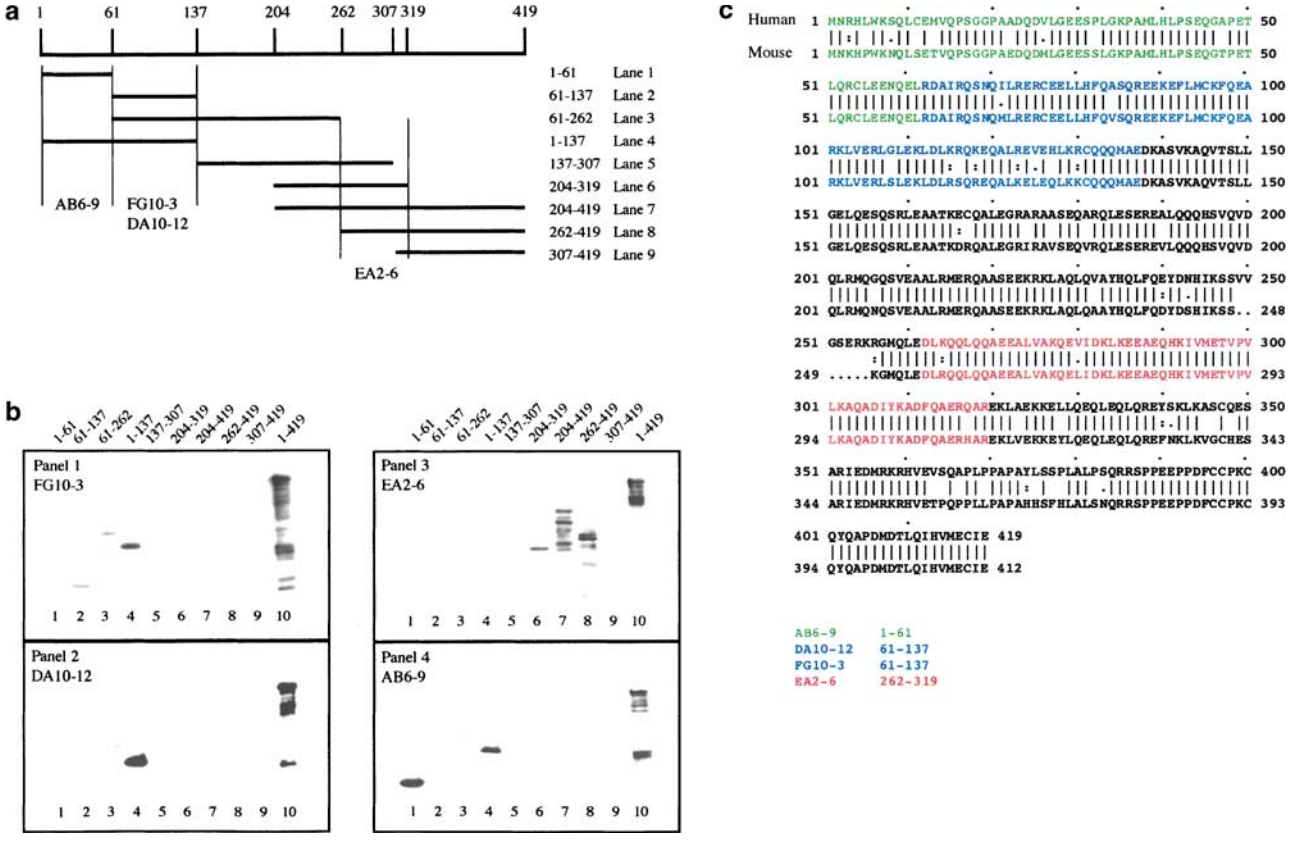

Figure 1 Characterization of four anti-NEMO mAbs. GST fusions of human NEMO were expressed and probed with the four mAbs in order to map the recognition regions. (**a**) Schematic representation of the GST-NEMO fragments used in Western blotting. (**b**) Western blotting of GST fusion proteins. Proteins were bound to glutathione–sepharose beads and eluted with 10 mM reduced glutathione, electrophoresed on 10% SDS–PAGE, and probed with either FG10-3 (panel 1), DA10-12 (panel 2), EA2-6 (panel 3), or AB6-9 (panel 4) mAb. Multiple bands are a result of protein degradation. (**c**) Alignment of mouse and human NEMO sequences. Regions that are deductively recognized by the four mAbs are in color: AB6-9 is shown in green, DA10-12 and FG10-3 are shown in blue, and EA2-6 is shown in red

2, lanes 2 and 3). A third clone, AB6-9 (Figure 1b, panel 4, lanes 1 and 4), recognized a separate N-terminal epitope located in amino acids 1–61, while the fourth clone, EA2-6, recognized three NEMO subfragments, 204–319, 204–419, and 262–419 (Figure 1b, panel 3, lanes 6–8). These results permitted the deduction of the minimal regions needed for recognition by each of the four mAbs (summarized in Figure 1c).

We also checked the reactivity of our monoclonals to mammalian cell-endogenous NEMO. (Similar results were seen with all four monoclonals; representative EA2-6 data are presented in Figure 2.) We first compared wild-type mouse embryo fibroblast (E6i) to the counterpart fibroblast from NEMO−/− knockout mouse (E8i). Cells, in parallel, were fixed, incubated with anti-NEMO monoclonal, and visualized by confocal microscopy using FITC-conjugated anti-mouse secondary antibody (Figure 2a). When compared to nuclear staining using 4,6-diamidino-2-phenylindole (DAPI), NEMO presented as fine cytoplasmic granules in NEMO+/+, but not NEMO−/−, fibroblasts (Figure 2a). Next, we immunoblotted human epithelial

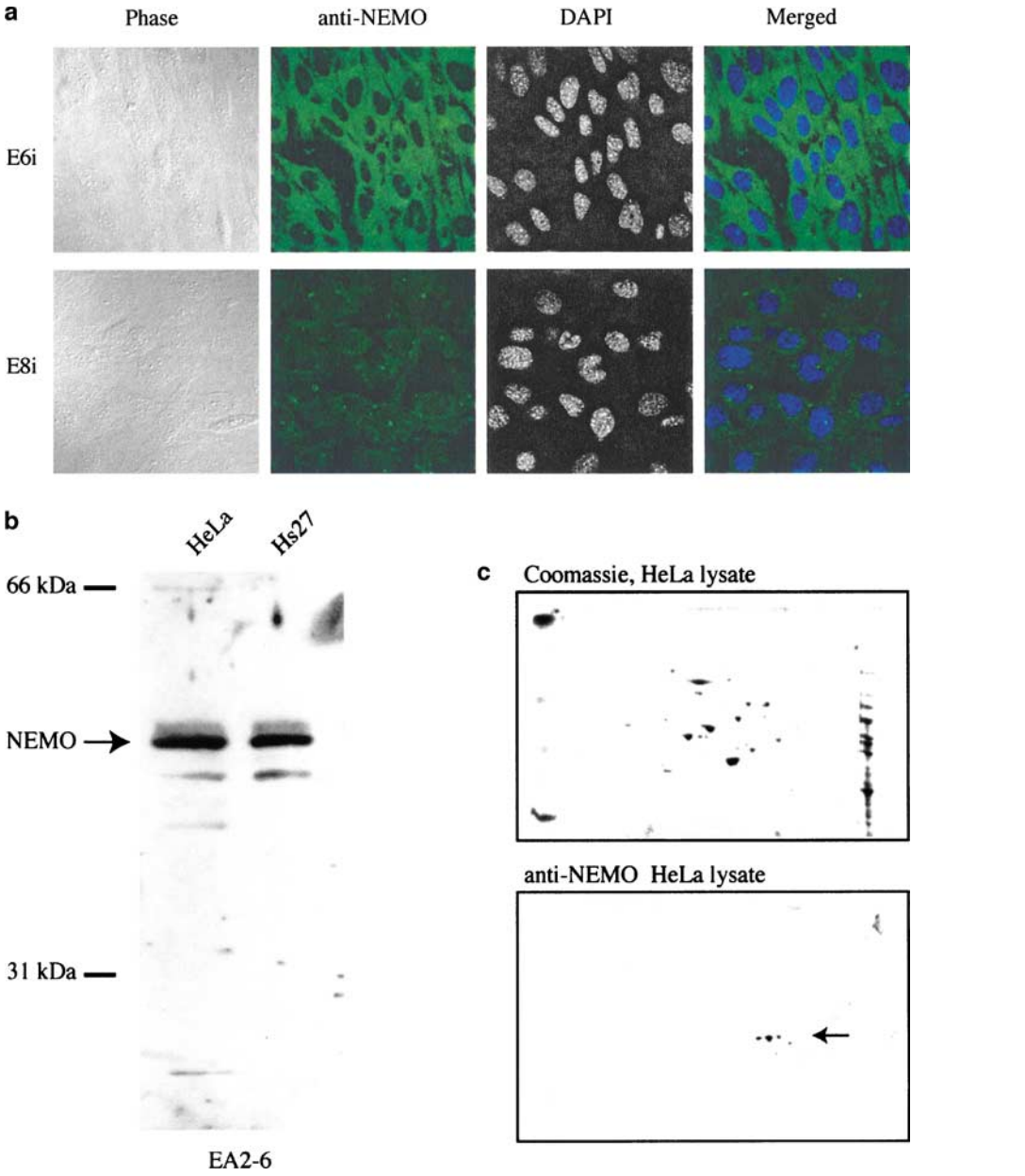

Figure 2 Recognition specificity of monoclonal EA2-6 for mammalian NEMO. (**a**) Immunofluorescent detection of NEMO in mouse cells. E6i MEF is wild type for NEMO; E8i MEF is genetically knocked-out for NEMO. Images shown (from left to right) are phase-contrast, indirect immunofluorescence with monoclonal EA2-6, DAPI, and overlay of EA2-6 with DAPI. Wild-type NEMO after fixation does not exhibit the prominent speckling seen with unfixed protein in living cells (see Figure 8). (**b**) Western blotting of human epithelial (HeLa) and human foreskin fibroblast cells with EA2-6. (**c**) Isoelectric focusing detection of human NEMO by EA2-6. HeLa lysate was first separated on a pH gradient (range shown is pH 4–7, left to right), and then separated by PAGE in 10% gels. (Top) 2-D gel stained with Coomassie blue. (Bottom) 2-D gel probed with monoclonal EA2-6

(HeLa) or primary foreskin (Hs27) cells with EA2-6 and identified a ~50 kDa doublet (Figure 2b) that resolved into several discrete spots by two-dimensional isoelectric focusing (Figure 2c). These latter results are consistent with the specific recognition by our mAb of multiply phosphorylated forms of human NEMO (Prajapati and Gaynor, 2002; Tarassishin and Horwitz, 2001).

Our aim for the mAbs was to see if they could be used to target NEMO intracellularly , and whether such targeting could help us segregate interactions used by Tax from that used by TNFα for activating NF-κB. Toward this goal, we explored a cationic lipid-based protein-transfection system (Pro-Ject, Pierce) for introducing mAbs into HeLa cells (Figure 3). The conditions for ⩾50% 'pro-jection' into HeLa cells were first established using an FITC-tagged control mouse mAb (Figure 3a). We also found that plasmid DNA could be cointroduced into cells with similarly high efficiency when mixed with mAb and cationic lipid (data not shown).

We next asked whether mAbs directed against three different NEMO epitopes (1–61 (AB6-9), 61–137

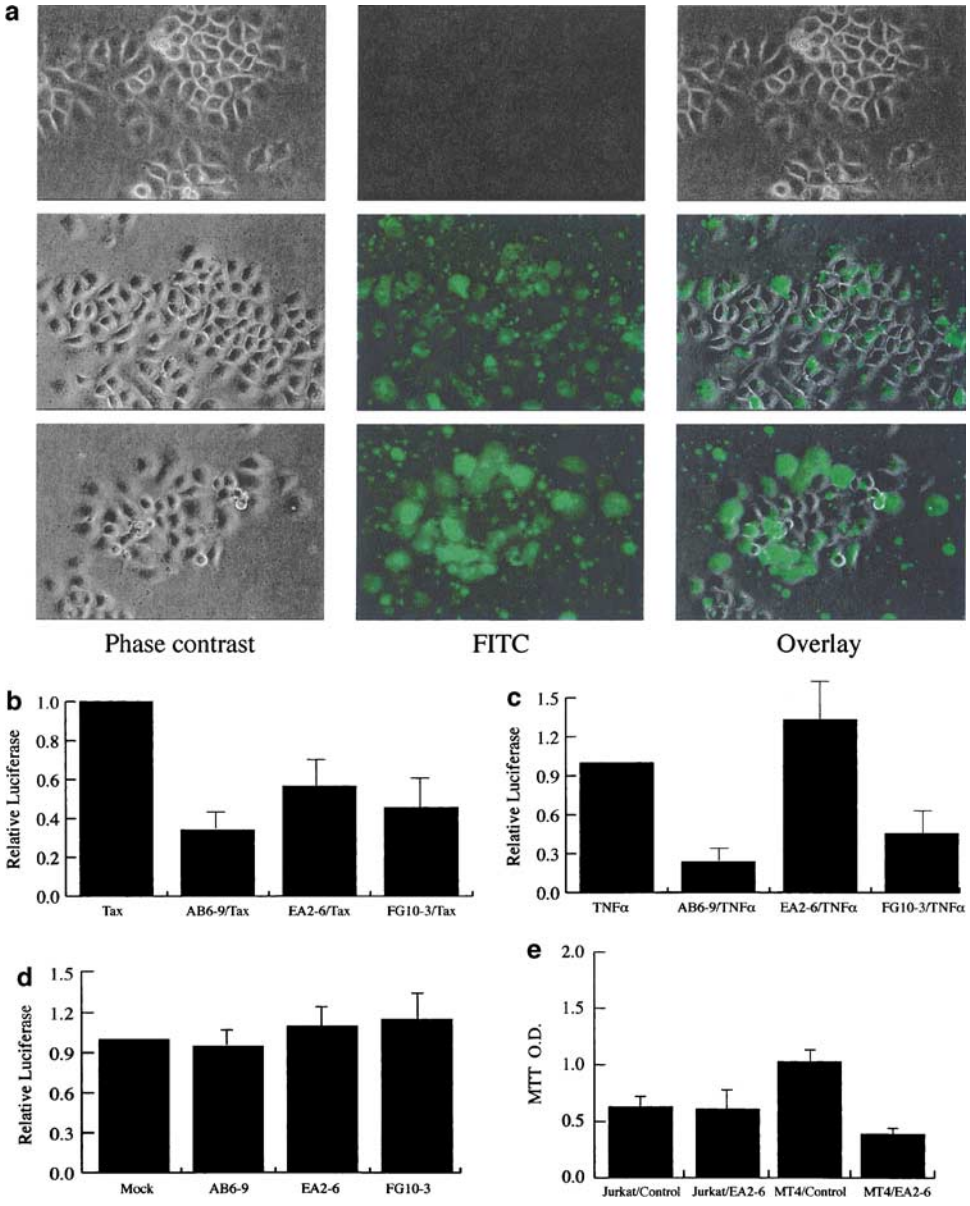

Figure 3 Protein transfection of anti-NEMO mAbs into human cells. (**a**) Transfection of fluorescent-tagged antibody into HeLa cells. Top row, mock transfection; middle and bottom rows, different views of the transfection of fluorescent-tagged mouse monoclonal into HeLa cells. Left column, phase-contrast views; middle column, green fluorescent views; right column, overlay of left and middle columns. (**b**) Transfection of HeLa cells with NF-κB-luc + Tax plasmid with control (Tax) and indicated mAbs. (**c**) Transfection of HeLa cells with NF-κB-luc + TNFα treatment with control (TNFα) and indicated mAbs. (**d**) Transfection of HeLa cells with AP-1 luciferase reporter and control (mock) and indicated mAbs. (**e**) Transfection of Jurkat or MT4 cells with control or EA2-6 antibodies. MTT values were assessed 48 h after transfection. Under the conditions used, protein transfection efficiencies approached ~50%. All bar graphs are averages from quadruplicate assays

(FG10-3), and 262–319 (EA2-6)) would segregate intracellular activation of NF-κB by Tax versus TNFα. We separately mixed each mAb with a Tax expression plasmid and an NF-κB-luciferase reporter (NF-κB-luc), and introduced them all together into cells. Luciferase activities were assayed 16 h later. In Tax cells, all three monoclonals (AB6-9, EA2-6, and FG10-3; Figure 3b, lanes 2–4) consistently inhibited the activation of NF-κB by 50–70% (Figure 3b, lane 1). On the other hand, TNFα-treated cells offered a different picture. Here, while AB6-9 and FG10-3 (Figure 3c, lanes 2, 4) inhibited NF-κB activity by 60–75%, EA2-6 (Figure 3c, lane 3) actually enhanced activity by approximately 25%. The magnitudes of these effects are comparable to the previously reported ~3-fold inhibition achieved with cell-permeable peptides targeted to NEMO (May *et al*., 2000).

To verify the specificity of our finding for Tax/NF-κB, we performed two additional controls. We 'pro-jected' our NEMO mAbs into cells with an AP-1-responsive reporter expressing significant basal luciferase activity. When luciferase activities were assayed 16 h later, we observed no perturbation of reporter expression with any of the monoclonals (Figure 3d). Next, we 'pro-jected' Tax-specific EA2-6 mAb in parallel separately into an HTLV-I-transformed T-cell (MT4) or a control T-cell line (Jurkat). We reasoned that should the EA2-6 effect be Tax specific and should proliferation of MT4 be driven by Tax activation of NF-κB, then growth of MT4, but not Jurkat, might be affected. Indeed, based on quadruplicate MTT readouts, EA2-6 selectively reduced the proliferation of MT4 cells (Figure 3e). Collectively, these results support the specificity of the observed Tax/TNFα/NF-κB findings (Figure 3b, c), ruling out trivial consequences of cellular toxicity (Figure 3d).

Different requirements for NEMO coimmunoprecipitation with IKKα/β and association with HMW intracellular IKK

The different antibody inhibition profiles suggested nonidentical interactions between Tax and TNFα with NEMO. We attempted to confirm this notion through a more conventional approach using NEMO mutants that might distinguish Tax from TNFα activation of NF-κB. Commencing with the coiled-coil (six putative coils, CC1 to CC6; Figure 4a) full-length 419 amino-acid human NEMO protein, we generated 10 serial deletion mutants, each tagged at their N-terminus with a FLAG epitope (Figure 4b). All mutants were confirmed by immunoblotting (IB) with anti-FLAG to express comparably when transfected into human cells (Figure 4c).

As a first characterization step, we tested the respective capacity of the NEMO mutants to co-immunoprecipitate (co-IP) IKKα and IKKβ. HA-tagged wild-type NEMO, HA-tagged IKKβ or HA-tagged IKKα was transfected into 293T cells with an individual FLAG-tagged NEMO mutant (Figure 5a). Cell lysates were immunoprecipitated with anti-FLAG, and co-precipitated protein(s) was detected by IB with

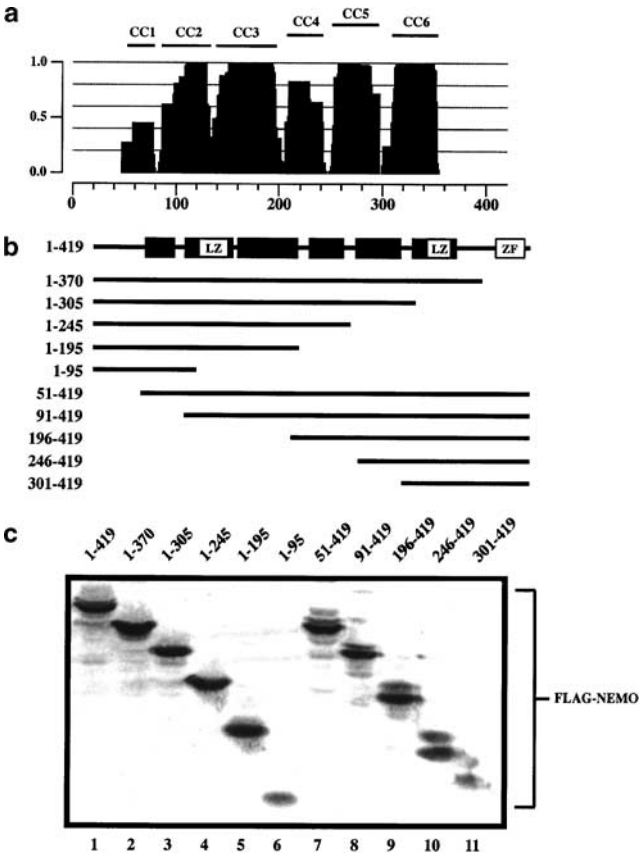

Figure 4 Construction and characterization of 10 NEMO mutants. (**a**) Schematic representation of the predicted coiled-coil structure of human NEMO (419 amino acids). The six coiled coils, predicted by MacStripe 2.0 (window 21), are indicated by bars (CC1-CC6) and shown in the solid plot. The *y*-axis shows the probability (*P*) value between 0 and 1. The *x*-axis shows residues numbered from the N-terminus of the protein. Coiled-coils are as follows: CC1 48–80, CC2 87–134, CC3 140–197, CC4 209–242, CC5 254–298, and CC6 311–353; LZ = leucine zipper; ZF = zinc-finger (Jain *et al*., 2001). (**b**) Schematic representations of 10 NEMO mutants. (**c**) Expression of FLAG-NEMO and its truncation mutants in 293T cells. 293T cells were transfected with FLAG-NEMO vectors expressing full-length NEMO (lane 1) and mutants 1–370 (lane 2), 1–305 (lane 3), 1–245 (lane 4), 1–195 (lane 5), 1–95 (lane 6), 51–419 (lane 7), 91–419 (lane 8), 196–419 (lane 9), 246–419 (lane 10), and 301–419 (lane 11). A total of 40 μg of lysates were immunoblotted with anti-FLAG

anti-HA. FLAG-NEMO 1–419, 1–370, 1–305, 1–245, 1–195 and 51–419 co-IPed HA-IKKα and HA-IKKβ (Figure 5a, top, middle) mapping a minimal IKKα/β-binding region to the first three NEMO coiled coils (CC1, CC2, CC3; amino acids 51–195, Figure 4a). Interestingly, when we tested whether NEMO mutants oligomerize by checking whether FLAG-tagged NEMO would co-precipitate HA-tagged NEMO, we found that the FLAG 1–419, 1–370, 1–305, 1–245, 51–419, 91–419, 196–419, and 246–419 proteins did precipitate HA-NEMO, while FLAG 1–95, 1–195, and 301–419 did not (Figure 5a, bottom). Thus, based on co-IPs, the N-terminal region NEMO (amino acids 51–195) co-IPed IKKα/β, while the central region (i.e. CC4 and CC5, spanning amino acids 196–300) self-co-IPed. Our current data (i.e. mutants 1–195 and 51–419; Figure 5a)

suggest that the N-terminus of NEMO recognizes IKKα and IKKβ identically in co-IPs. We have no explanation as to why these findings differ slightly from the co-IPs of Tegethoff *et al*. (2003), who reported a selective contribution by amino acids 1–65 of NEMO for binding IKKα, but not IKKβ. Co-IPs do not address whether the observed association between two proteins is a component of a larger multiprotein framework. As the biological form of cytokine-activated NF-κB kinase is a HMW 600–900 kDa complex (Chen *et al*., 1996; Mercurio *et al*., 1997; Zandi *et al*., 1997; Rothwarf *et al*., 1998; Mercurio *et al*., 1999; Li *et al*., 2001), the relevant protein–protein interaction would be one which specifies an association with HMW IKK. Previous co-IP studies (Ye *et al*., 2000; Xiao *et al*., 2000) do not address clearly the portion of NEMO needed to coalesce with HMW IKK. Similarly, the converse binding requirement (i.e. whether the IKKα/β NEMO-binding domain, May *et al*., 2000, represents the sole region for recruiting NEMO into HMW IKK, Miller and Zandi, 2001) also remains unclear. Thus, in order to better understand physiological interactions, we interrogated our NEMO mutants for their intercalation into HMW cellular IKK.

We separately expressed FLAG-wild-type and five FLAG-NEMO mutants in HeLa cells. S100 lysates were prepared and chromatographed over a Superose 6 FPLC column (Figure 5b), and fractions were collected and aligned with molecular size standards. All samples were immunoblotted with anti-IKKα, anti-IKKβ, anti-NEMO, or anti-FLAG as indicated. Within the general resolution of this technique, we observed that the majority of two NEMO mutants, 1–95 and 301–419, chromatographed as low molecular weight (<232 kDa) entities that we interpret to be most consistent with protein monomers. By contrast, three other NEMO mutants 1–195, 1–245, and 246–419 distributed towards higher molecular weight fractions, a behavior more consistent with protein oligomers (Figure 5b, NEMO 1–95, 1–195, 1–245, 246–419, and 301–419). When cell-endogenous IKKα and IKKβ were analysed, these

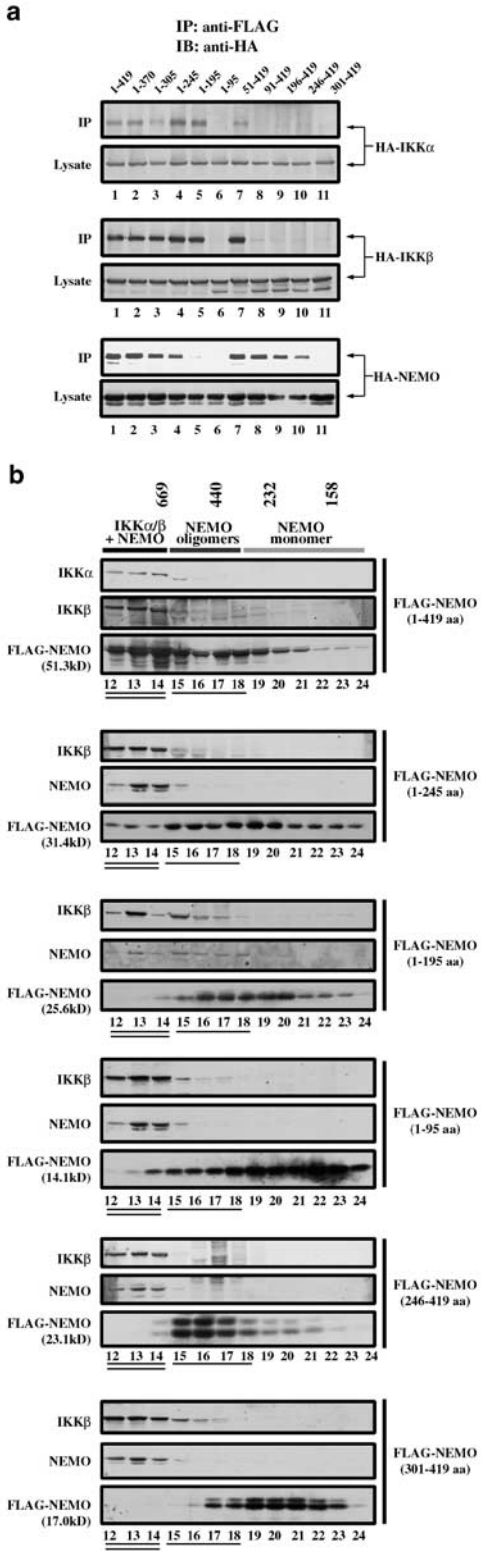

Figure 5 Characterization of the association between IKKα, IKKβ, and wild-type and mutant NEMO proteins by co-IP and chromatographic fractionation. (**a**) Co-IPs of IKKα and NEMO (top), IKKβ and NEMO (middle), and NEMO–NEMO self-interaction (bottom). 293T cells were transfected with HA-tagged IKKα (top), IKKβ (middle), and NEMO (bottom) expression vectors (all lanes) and FLAG-tagged NEMO vectors as shown in Figure 4c. A total of 100 μg of cell lysates were subjected to IP with 2 μg of mouse monoclonal anti-FLAG antibody (anti-FLAG), followed by IB with rabbit polyclonal anti-HA antibody (anti-HA) (upper panel). The transfection efficiency was verified by IB with anti-HA (lower panel). In each case, the expression of the FLAG-tagged NEMO was verified as shown in Figure 4c (data not shown). (**b**) Chromatographic fractionation of IKKα, IKKβ, and NEMO. HeLa cells were transfected with FLAG-tagged NEMO expression vectors (10 μg) and 2 mg of the S100 cytoplasmic extracts (see Experimental procedures) were subjected to Superose 6 column chromatography. The amino acids length of FLAG-tagged NEMO and its mutants are indicated to the right-hand side of each panel. Fractions from 12 to 24 (30 μg each lane) were resolved with either 10% (FLAG-NEMO 1–419, 1–245, 1–195, and 246–419) or 12% (FLAG-NEMO 1–95 and 301–419) SDS–PAGE and probed with anti-FLAG, mouse monoclonal anti-IKKα, anti-IKKβ, and anti-NEMO antibodies. The position of the molecular weight markers (669, 440, 232, and 158 kDa) and the numbers of the column fractions are indicated. Double-underlined numbers indicate fractions containing HMW IKKα/β/ NEMO complex; single-underlined numbered fractions are compatible with NEMO/ NEMO oligomers

partitioned consistently into >669 kDa fractions (Figure 5b); similarly, FLAG-full-length NEMO also distributed into these fractions (Figure 5b, FLAG-NEMO 1–419). On the other hand, when we checked for the presence of NEMO mutants in the >669 kDa region, we found approximately 15% of FLAG-NEMO 1–245 fractionated there, while less than 1% of mutants 1–95, 1–195, 246–419, or 301–419 was detected in the HMW fractions (Figure 5b, FLAG-NEMO 1–95, 1–245, 246–419, 301–419). Hence, in distinction with co-IP results that showed that NEMO 1–245 and full-length 1–419 protein precipitated IKKα/β indistinguishably (Figure 5a), the chromatographic evidence indicated that NEMO 1–245 mutant, in the context of an HMW complex, associated less efficiently than full-length NEMO with cellular holo-IKK (Figure 5b). Altogether, the chromatographical results suggest that amino acids C-terminal to position 95 of NEMO participates in oligomerization and that oligomerization, while seemingly unnecessary for co-IP with IKKα/β, appears to be critical for NEMO to participate in intracellular HMW IKK complex formation.

Different NEMO domains participate in cytokine- and tax-induced NF-κB activation

We next checked whether our NEMO mutants could distinguish between Tax versus cytokine activation of NF-κB. As a first step, we employed NEMO knockout mouse embryonic fibroblasts (E8i cells, Schmidt-Supprian *et al*., 2000) to check for functional complementation. NEMO is essential for the activation of NF-κB by TNFα, IL-1β, or Tax (Chu *et al*., 1999: Harhaj and Sun, 1999; Jin *et al*., 1999; Makris *et al*., 2000; Rudolph *et al*., 2000; Schmidt-Supprian *et al*., 2000). As expected, in E8i cells, NF-κB could not be activated by TNFα, IL-1β, or Tax (Figure 6; compare control lanes to TNFα, IL-1β, and Tax lanes). NF-κB activation by all three stimuli was uniformly rescued when full-length 1–419 NEMO was transfected into E8i cells (Figure 6, NEMO 1–419 lanes). When different mutants were tested, only three exhibited activity. Mutant 51–419 was reproducibly more active than wild-type NEMO, while mutant 1–370 was fully active for Tax and IL-1β, and less active for TNFα. A third mutant, 1–245, was completely inactive for TNFα and IL-1β, but was partially active for Tax (Figure 6). These complementation results support the antibody inhibition findings that proinflammatory cytokines and Tax signal nonidentically through NEMO.

To distinguish differences between TNFα and Tax more clearly, we wondered whether some of the loss-of-function NEMO mutants would exhibit differential dominant-negative phenotypes. We explored seven E8i noncomplementing mutants, NEMO 1–95, 1–195, 1–305, 91–419, 196–419, 246–419, and 301–419, in NEMO+/+ E6i cells. Interestingly, when these mutants were checked for dominant-negative activity

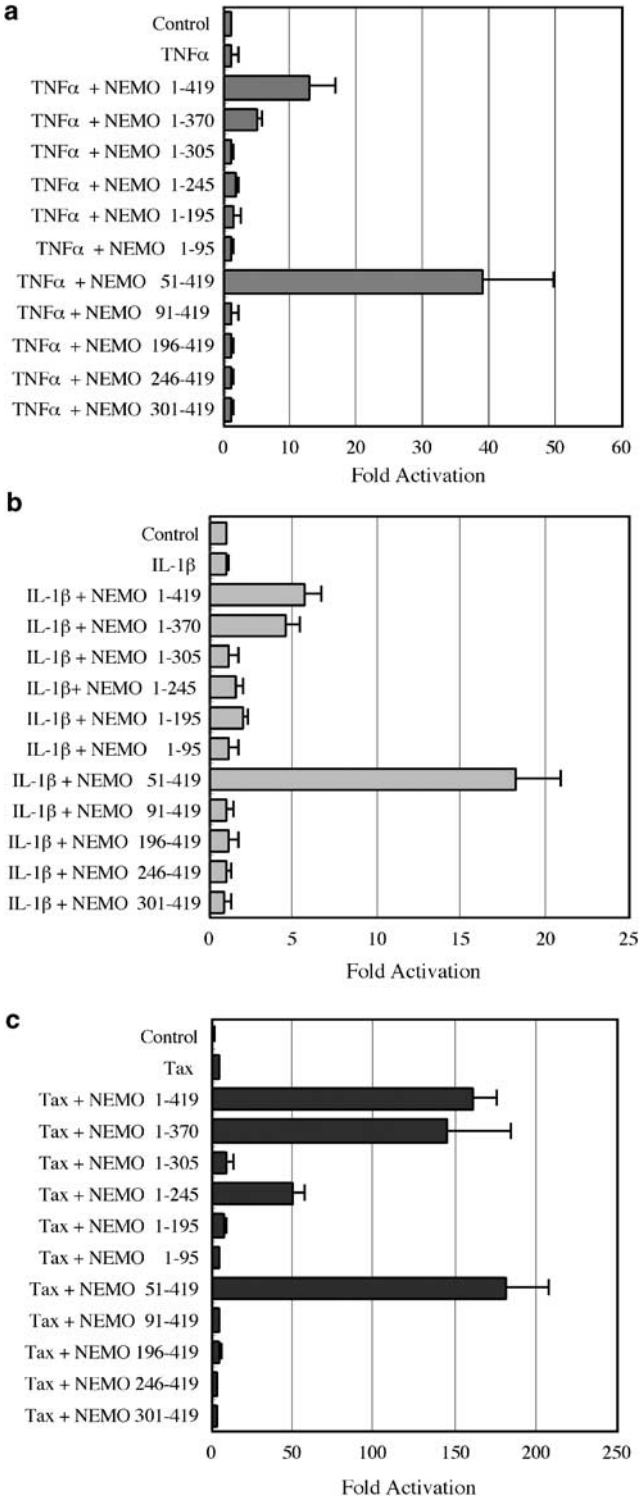

Figure 6 NEMO domains required for functional complementation of cytokine- or Tax-induced NF-κB activation. Mouse NEMO knockout E8i cells were transfected with 1 μg of total DNA containing a mixture of 100 ng of NF-κB-luc (Stratagene) with 100 ng of RSV-β-galactosidase, 10 ng of the indicated NEMO expression vectors, with or without 250 ng of the Tax expression vector and with the appropriately balanced amounts of carrier DNA. After 16 h of transfection, TNFα (2 ng/ml, **a**) and IL-1β (1 ng/ml, **b**) were added and incubated for 8 h. Cells were harvested for luciferase assay 24 h after transfection. Fold activation was based on the division of normalized luciferase values after activation by the normalized basal luciferase values

against TNFα, only 1–305 exhibited significant inhibition (Figure 7a). By contrast, four mutants, 1–195, 1–305, 91–419, and 196–419, suppressed Tax activity (Figure 7b). Thus, the different dominant-negative patterns further confirm (Figures 3 and 6) that TNFα and Tax work through separate NEMO domains.

We were puzzled that most of our mutants failed to inhibit TNFα signaling. All mutants expressed robustly in cells when assayed by IB (Figure 4 and data not shown), suggesting that their lack of activity against TNFα cannot be explained by deficient intracellular synthesis. However, the mutants could possibly be misfolded or misdistributed intracellularly. To investigate this possibility, we constructed 10 green fluorescent forms of NEMO and checked their respective presentations in living cells (Figure 8). When expressed in mouse embryo fibroblasts, wild-type GFP-NEMO (Figure 8, 1–419) was nuclearly excluded and appeared as multiply discrete rounded cytoplasmic speckles. When N-terminal sequences were deleted progressively, the 51–419 and 91–419 proteins maintained the round cytoplasmic speckles (Figure 8; 51–419, 91–419); however, the 196–419, 246–419 mutants (Figure 8; 196–419, 246–419) lost their speckled organization, albeit their fluorescence remained cytoplasmic. When GFP-fused C-terminally deleted NEMO proteins were viewed, three, 1–195, 1–245, and 1–370, showed finely granulated cytoplasmic fluorescence. GFP-1–95, probably because of its small size, was distributed into both the nucleus and cytoplasm, while GFP-1–305, which is essentially identical to the previously described IKKγΔC molecule (Rothwarf *et al*., 1998) consistently coalesced into large cytoplasmic aggregates (Figure 8, 1–305). To the extent that cytoplasmic speckling represents the correct folding/configuration of wild-type NEMO in a GFP-live-cell context, our results suggest that most mutants show some misfolding. That only one (i.e. 1–305) mutant is dominant negative for TNFα while four others could suppress Tax activity is compatible with different folding/structural requirements for NEMO to interact with the former versus the latter. These results further highlight the differences between Tax and TNFα in their respective activation of NF-κB through NEMO.

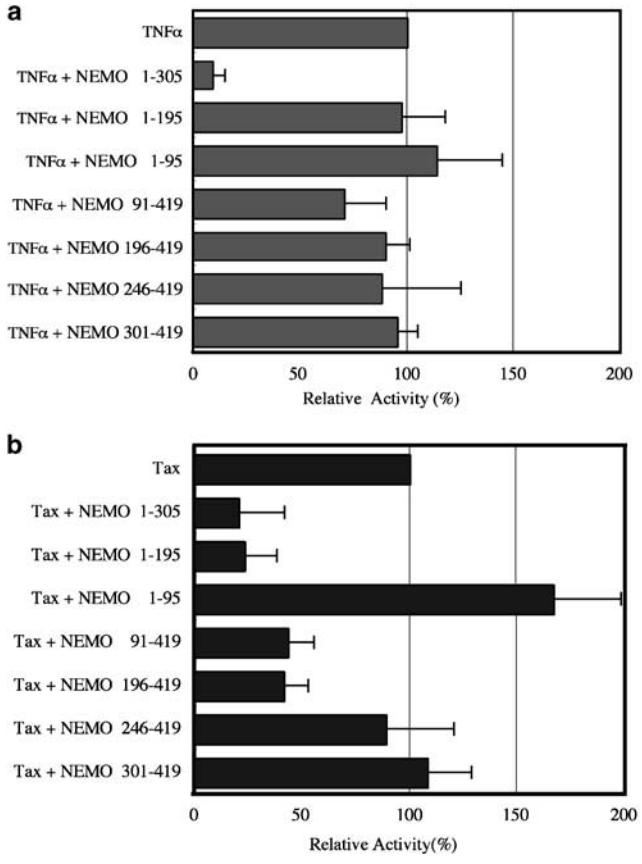

Figure 7 Domain-specific inhibition of cytokine-induced or Tax-mediated NF-κB activation by NEMO mutants. Mouse E6i cells were transfected with 1 μg of plasmid DNA containing 100 ng of NF-κB-luc (Stratagene) and 100 ng of RSV-β-galactosidase, with 100 ng (**a**) or 500 ng (**b**) of the indicated NEMO expression vector, and with or without 250 ng of the Tax expression vector. After 16 h of transfection, TNFα (2 ng/ml, **a**) was added and incubated for 8 h. Cells were harvested for luciferase assay after 24 h of transfection. The amino acids retained in each of the NEMO mutants are indicated to the left-hand side of each column

Discussion

NF-κB activity contributes to multiple biological processes including cell growth, cellular transformation and cell death (Beyaert *et al*., 2000; Karin and Lin, 2002; Li and Verma, 2002). The HMW holo-IKK complex has been shown to be the critical biologically relevant kinase for NF-κB activation. Current thinking suggests that most, if not all, IKK-activating signals transits through the IKK-adaptor subunit NEMO. In this regard, both transformation of cells by HTLV-I oncoprotein, Tax (Nerenberg *et al*., 1987; Grassmann *et al*., 1989; Tanaka *et al*., 1990), and cellular activation by proinflammatory cytokine, TNFα, have been shown to require NEMO. Genetic data from knockout mice (Makris *et al*., 2000; Rudolph *et al*., 2000; Schmidt-Supprian *et al*., 2000) have firmly established the physiological importance of NEMO for NF-κB activation by various signals. However, how NEMO is contacted by and responds to the variously converging signals remains incompletely elucidated. Here, using TNFα and Tax as two types of NEMO-activating stimuli, we show that the oncogenic and proinflammatory signals impinge upon different and separable domains of NEMO/IKKγ.

Tax is unambiguously the cellular transforming factor for HTLV-I (Yoshida, 2001; Marriott *et al*., 2002). The activation of NF-κB by Tax has been proposed as a causal viral mechanism for ATL (Ballard *et al*., 1988; Kitajima *et al*., 1992; Mori *et al*., 1994; Robek and Ratner, 1999; Tsukahara *et al*., 1999). Accordingly, although it has yet to be contemplated, ATL therapy, in principle, would benefit from interruption of NF-κB activation. However, global inhibitory approaches using nonsteroidal anti-inflammatory drugs and/or immunosuppressive agents (Yamamoto and Gaynor, 2001) may be counterproductive, since such routes could abrogate NF-κB's oncogenic potential at the expense of blocking

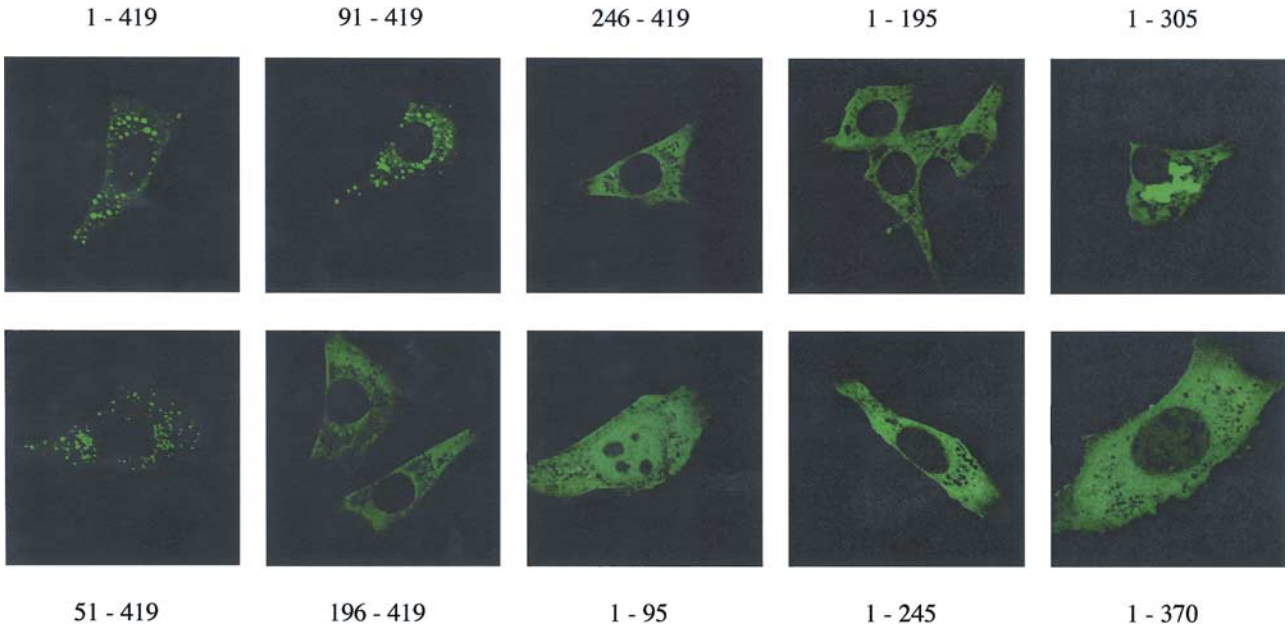

Figure 8 Green fluorescent presentations of full-length human NEMO and nine truncation mutants in living cells. HeLa cells were transfected with GFP-1–419, 51–419, 91–419, 196–419, 246–419, 1–95, 1–195, 1–245, 1–305, and 1–370. Cells were visualized 24 h later

other NF-κB activities needed for normal cellular metabolism. As NEMO is a nexus at which many diverse signals converge, should one capably delineate discrete domains that subserve different types of signaling, then stimulus-specific interruption of NF-κB-activation through targeting of NEMO might be practically feasible (Li *et al*., 1999c; Zhang *et al*., 2000; Orlowski and Baldwin, 2002).

By introducing three independent mAbs into cells, we provide the first evidence that oncogenic and proinflammatory signaling through NEMO can be independently interrupted (Figure 3). Our approach builds upon the confluence of three emerging technologies: (i) the increasing efficacious use of mAbs in treating human pathologies (Ranson and Sliwkowski, 2002; Ghosh *et al*., 2003), (ii) the finding that single-chain intracellular antibodies can effectively inhibit the function of cellular factors (Bai *et al*., 2003), and (iii) the advent of commercially available high-efficiency protein-transfection reagents. Our intracellular antibody data provided two salient insights. First, the results confirmed in living cells the importance of the N-terminus of NEMO for contact with IKKα/β (May *et al*., 2000; Poyet *et al*., 2000; Ye *et al*., 2000) and the common role that this interaction serves for Tax and TNFα activation of NF-κB. Second, the findings indicate that the central region of NEMO (i.e. amino acids 262–319) functions differently for Tax versus TNFα. Hence, the EA2-6 mAb inhibited Tax activation, while it enhanced TNFα activation (Figure 3). Other explanations not excluded, one interpretation is that the EA2-6 may have a blocking as well as a stabilizing function for NEMO. This antibody may sterically obstruct the interaction between Tax and NEMO amino acids 304–339 (Xiao *et al*., 2000), thereby perturbing activation. On the other hand, EA2-6 through its overlapping interaction with amino acids 242–388 or 246–365 could possibly stabilize NEMO trimerization/tetramerization (Agou *et al*., 2002; Tegethoff *et al*., 2003) leading to enhanced TNFα responsiveness. Additional physical studies are pending in order to confirm these reasonings.

To further investigate the notion that TNFα and Tax signal differently, we also created 10 function-retaining or loss-of-function NEMO mutants (Figures 4, 6 and 7). The 10 mutants yielded instructive findings regarding structured domains required for NEMO function. Initially, in co-IPs, we found, as expected from previous reports (May *et al*., 2000; Poyet *et al*., 2000; Ye *et al*., 2000), that amino acids 1–195 and 196–245 described minimal NEMO domains needed, respectively, for co-precipitating IKKα/β and for self-co-precipitation (Figure 5a). Intriguingly, when we further asked as to what portion of NEMO was needed for association with HMW (>669 kDa) cellular holo-IKK, a more complicated scenario emerged. In this context, full-length NEMO intercalated efficiently, while NEMO 1–245 intercalated partially into HMW IKK (Figure 5b). On the other hand, neither NEMO 1–195, 246–419 nor 301–419 could be detected with HMW IKK (Figure 5b). Hence, different from that required for NEMO to co-IP IKKα/β, both the 1–195 (contact) and the sequences C-terminal to 196 (oligomerization region) are needed for a biologically relevant association of NEMO with intracellular HMW IKK. This conclusion supports recent proposals that trimerization/tetramerization of NEMO is important for function (Poyet *et al*., 2000; Agou *et al*., 2002; Huang *et al*., 2002; Tegethoff *et al*., 2003) and suggests that NEMO oligomerization is a functional prerequisite for its association with HMW IKK.

Two additionally unexpected findings emerged from our complementation and dominant-negative experi-

ments (Figures 6, 7). First was the observation that NEMO 1–245 supported Tax activation (Figure 6). That NEMO 1–245 could complement Tax in E8i cells was surprising, since previously it was argued that mouse NEMO sequences spanning 304–339 were required to bind Tax in co-IP assays (Xiao *et al*., 2000). Recently, when this issue was re-examined, others (Huang *et al*., 2002) and we (Iha, data not shown) found that Tax actually bound the 201–250 region of human NEMO directly. Thus, while sequence 304–339 may contribute an important conformational influence on NEMO function (Figure 3), it is the NEMO sequence upstream of position 245 that represents the direct Tax-binding target. In the context of the above finding, a second curios finding was that mutant 1–305 failed to support Tax function (Figure 6) and, in fact, dominantly inhibited both TNFα and Tax activation of NF-κB (Figure 7). Human NEMO mutant 1–305 is essentially identical to the prevalently used dominant-negative mouse IKKγΔC previously described elsewhere (Rothwarf *et al*., 1998). It was perplexing that human NEMO 1–245 provided partial complementation, while human NEMO 1–305 was dominant negative. However, when we visualized GFP-NEMO 1–305 in living cells, it, unlike any other mutant that we surveyed, formed unusual cytoplasmic aggregates (Figure 8). This particular presentation could explain why NEMO 1–305 dominantly inhibited TNFα activation of NF-κB, while other loss-of-function mutants in our assays showed no comparable inhibitory activity (Figure 7). Of interest, we also noted that unfixed GFP-full-length NEMO in living cells showed prominent punctate cytoplasmic speckles (Figure 8, 1–419) reminiscent of that previously described for FKBP12-enforced oligomerization/trimerization of a chimeric GFP-IKKγ-truncated protein (Figure 6 in Poyet *et al*., 2000). This observation suggests that some amount of native NEMO (as well as mutant proteins that contain sequences from 91 to 419) may constitutively exist as oligomers/trimers without requiring stimulus induction (Figure 8). By contrast, partially active mutants such as 1–245 may be constitutively oligomerization inefficient, but can be driven to oligomerize by the appropriate cofactors and stimuli (Huang *et al*., 2002).

Finally, the key message of our study is the discrete segregation of NEMO domains used by Tax and TNFα. Future studies remain necessary to clarify the NEMO-downstream mechanistic differences between Tax and TNFα for NF-κB activation. Nevertheless, as an initial step towards better therapeutic applications, we are encouraged that intracellular antibody targeting the NEMO 262–319 region can regress the proliferative growth of Tax-transformed T-leukemic cells without toxicity for control T cells (Figure 3). Conceivably, cell-permeable peptides (May *et al*., 2000) targeting this portion of human NEMO might provide novel-specific adjuncts to conventional ATL therapy. Alternatively, an EA2-6 Fab fragment fused to a protein-transduction domain could possibly be therapeutic for ATL. Future investigations following these lines of thought appear to be warranted.

Materials and methods

Prediction of coiled-coil structure on human NEMO

The coiled-coil domains of human NEMO were predicted by MacStripe 2.0 version with the window size of 21 (Lupas *et al*., 1991).

Cells and cell-culture conditions

Immortalized mouse embryonic cell, E6i and its NEMO knockout counterpart E8i, were a kind gift from Dr Marc Schmidt-Supprian; (Schmidt-Supprian *et al*., 2000), Hs27 (primary human foreskin fibroblast), 293T, HeLa, MT4, and Jurkat cell lines were obtained from ATCC. All adherent cells were cultured in complete DMEM/high glucose with 10% fetal bovine serum. Suspension cells were cultured in complete RPMI-1640 supplemented with 10% FBS. The cell proliferation assay with a modified MTT dye reduction assay was as previously described (Kasai *et al*., 2002).

Plasmids

IKKα, IKKβ, NEMO, and Tax were amplified from vectors previously described (Mercurio *et al*., 1997; Jin *et al*., 1999; Ng *et al*., 2001) and cloned into pcDNA3 (Invitrogen). GFP-NEMO expression vectors were cloned into pEGFP-C3 (Clontech). pGEX-IKKγ was previously described (Jin *et al*., 1999). Other GST-NEMO fusion fragments were cloned into pGEX-4T1 (Amersham Pharmacia Biotech). All vectors were verified by sequencing.

Co-IP and IB

A total of 1×10^6 cells of 293T were transfected with 1 μg of each plasmid by TransIT LT1 (Mirus). After 24 h, cells were lysed (0.5% Nonidet P-40, 50 mM HEPES (pH 7.3), 150 mM NaCl, 2 mM EDTA, 1 mM phenylmethylsulfonyl fluoride (PMSF), 0.1 mM sodium orthovanadate (Na_3VO_4), 1 mM sodium fluoride (NaF), 10% glycerol and protease inhibitor mix (Roche)). In all, 100 μg of lysates were precleared with 30 μl of protein G/A agarose (Oncogene Research Products) for 2 h and incubated with 2 μg of mouse monoclonal anti-FLAG antibody (M2, Sigma) and 30 μl of protein G/A agarose for at least 3 h at 4°C. Antibody–agarose complexes were washed 3 × with lysis buffer, resolved by 10 or 12% SDS–poly acrylamide gel electrophoresis (SDS–PAGE) and transferred onto a PVDF membrane (Millipore) using conditions previously described (Kibler and Jeang, 2001). HA-tagged IKKs were detected by rabbit polyclonal anti-HA antibody (Sigma); Tax, by anti-Tax mAbv from NIH AIDS Research Reference Reagent program.

FPLC protein fractionation and IB

Cytoplasmic extracts were prepared (Yamamoto *et al*., 2001) with slight modifications. A total of 1.6×10^7 of HeLa cells were transfected with 10 μg of pcDNA3 vectors expressing FLAG-NEMO or truncation mutants using Monster HeLa (Mirus) and harvested 24 h later. Cells washed 2 × with cold PBS were pelleted at 1500 r.p.m. for 5 min. Pellets were resuspended into buffer A (10 mM HEPES (pH 7.9), 1 mM EDTA, 10 mM KCl, 1 mM dithiothreitol (DTT)) supplemented with phosphatase inhibitors (50 mM NaF, 50 mM glycerol phosphate, 1 mM Na_3VO_4) and proteinase inhibitors. After incubation on ice for 15 min, cells were disrupted with 20 strokes through a 25-gauge needle and centrifuged at 16 000 *g* for 15 min. The supernatants were mixed with 0.11 volume of

buffer B (0.3 M HEPES (pH 7.9), 30 mM $MgCl_2$, 1.4 M KCl) and centrifuged at 100 000 *g* for 60 min. In total, 2 mg of supernatant (S100) were subjected to Superose 6 HR 10/30 (Amersham Pharmacia Biotech) chromatography in buffer D (20 mM HEPES (pH 7.9), 0.1 M KCl, 0.5 mM DTT, 0.5 mM PMSF, 20% glycerol, and 0.2 mM EGTA), and 0.9-ml fractions were collected. Protein markers (Amersham Pharmacia Biotech) were thyroglobulin (669 kDa), ferritin (440 kDa), catalase (232 kDa), aldolase (158 kDa), and bovine serum albumin (66 kDa). Proteins (30 μg) from fractions 12–24 in each chromatographic run were precipitated with TCA, subjected to 10 or 12% SDS–PAGE and detected with monoclonal anti-FLAG M2, monoclonal anti-IKKα and anti-IKKβ antibodies (Oncogene Research Products), or monoclonal anti-NEMO.

Luciferase assay

The transfection of cells was as previously described (Iha *et al*., 2000). Briefly, 1×10^5 cells of E6i and E8i were transfected with 1 μg of plasmid DNA mixture containing reporter plasmids, 100 ng of NF-κB-luc (Stratagene) and 100 ng of RSV-β-galactosidase, by TransIT LT1. The total DNA was normalized by the addition of pcDNA3. After 16 h, where indicated, mouse TNFα (Calbiochem) or IL-1β (Sigma) at concentrations of 2 or 1 ng/ml, respectively, were added for 8 h. Luciferase was measured 24 h after transfection in an Opticom II luminometer (MGM Instruments). Cell extracts used for luciferase assay were quantitated for β-galactosidase activity using Galacto-Star (Tropix), and normalized based on β-galactosidase readings.

Confocal microscopy

E6i cells were cultured on 25 mm coverslips (Thomas Scientific) and transfected with 500 ng of GFP-NEMO plasmid. Cells were fixed with 3.7% formaldehyde and stained with DAPI (Molecular Probes). Coverslips were mounted onto glass slides with a ProLong Antifade Kit (Molecular Probes) and examined with a Leica DM IRBE laser-scanning microscope (Iwanaga *et al*., 2002).

mAb production and transfection into cells

Balb/C mice were injected with purified GST-IKKγ. Spleen cells of positive mice were cultured with NSI myeloma cells (ATCC), individual hybridomas were isolated, clone supernatants were screened by ELISA, Western blotting, and immunoprecipitation. Ascites were produced in mice (Spring Valley, Woodbine, MD, USA). The IgG isotype was determined with Mouse Typer Sub-Isotyping Kit (Bio-Rad) according to the manufacturer's instructions; all four clones are IgG_1. For the transfection of antibody into cells the Project Protein Transfection Reagent Kit (Pierce) was used according to the manufacturer's protocol.

Isoelectric focusing

Separation was performed in the PROTEAN IEF Cell system (BioRad) according to the manufacturer's instructions. Proteins bound to immobilized pH gradient gel strips were then electrophoresed in 10% precast polyacrylamide gels (BioRad).

Acknowledgements
We are indebted to Marc Schmidt-Supprian for NEMO knockout cells. We thank Shao-Cong Sun for plasmids, Alicia Buckler-White for sequencing, George Dapolito for technical assistance, and Dong-Yan Jin for reading the manuscript.

References

Agou F, Ye F, Goffinont S, Courtois G, Yamaoka S, Israel A and Veron M. (2002). *J. Biol. Chem.,* **277,** 17464–17475.
Bai J, Sui J, Zhu RY, Tallarico AS, Gennari F, Zhang D and Marasco WA. (2003). *J. Biol. Chem.,* **278,** 1433–1442.
Ballard DW, Bohnlein E, Lowenthal JW, Wano, Franza BR and Greene WC. (1988). *Science,* **241,** 1652–1655.
Beyaert R, Heyninck K and Van Huffel S. (2000). *Biochem. Pharmacol.,* **15,** 1143–1151.
Chen ZJ, Parent L and Maniatis T. (1996). *Cell,* **84,** 853–862.
Chu ZL, Shin YA, Yang JM, DiDonato JA and Ballard DW. (1999). *J. Biol. Chem.,* **274,** 15297–15300.
Courtois G, Smahi A and Israel A. (2001). *Trends Mol. Med.,* **7,** 427–430.
Courtois G, Whiteside ST, Sibley CH and Israel A. (1997). *Mol. Cell. Biol.,* **17,** 1441–1449.
DiDonato JA, Hayakawa M, Rothwarf DM, Zandi E and Karin M. (1997). *Nature,* **388,** 548–554.
Ghosh S, Goldin E, Gordon FH, Malchow HA, Rask-Madsen J, Rutgeerts P, Vyhnalek P, Zadorova Z, Palmer T, Donoghue S and Natalizumab Pan-European Study Group. (2003). *N. Engl. J. Med.,* **348,** 24–32.
Grassmann R, Dengler C, Muller-Fleckenstein I, McGuire K, Dokhelar MC, Sodroski JG and Haseltine WA. (1989). *Proc. Natl. Acad. Sci. USA,* **86,** 3351–3355.
Harhaj EW and Sun SC. (1999). *J. Biol. Chem.,* **274,** 22911–22914.
Hinuma Y, Nagata K, Hanaoka M, Nakai M, Matsumoto T, Kinoshita KI, Shirakawa S and Miyoshi I. (1981). *Proc. Natl. Acad. Sci. USA,* **78,** 6476–6480.
Hu Y, Baud V, Delhase M, Zhang P, Deerinck T, Ellisman M, Johnson R and Karin M. (1999). *Science,* **284,** 316–320.
Huang GJ, Zhang ZQ and Jin DY. (2002). *FEBS Lett.,* **531,** 494–498.
Iha H, Kasai T, Kibler KV, Iwanaga Y, Tsurugi K and Jeang KT. (2000). *AIDS Res. Hum. Retroviruses,* **16,** 1633–1638.
Iwanaga Y, Kasai T, Kibler K and Jeang KT. (2002). *J. Biol. Chem.,* **277,** 31005–31012.
Jain A, Ma CA, Liu S, Brown M, Cohen J and Strober W. (2001). *Nat. Immunol.,* **2,** 223–228.
Jin DY, Giordano V, Kibler KV, Nakano H and Jeang KT. (1999). *J. Biol. Chem.,* **274,** 17402–17405.
Karin M. (1999). *J. Biol. Chem.,* **274,** 27339–27342.
Karin M, Cao Y, Greten FR and Li ZW. (2002). *Nat. Rev. Cancer,* **2,** 301–310.
Karin M and Lin A. (2002). *Nat. Immunol.,* **3,** 221–227.
Kasai T, Iwanaga Y, Iha H and Jeang KT. (2002). *J. Biol. Chem.,* **277,** 5187–5193.
Kibler KV and Jeang K-T. (2001). *J. Virol.,* **75,** 2161–2173.
Kitajima I, Shinohara T, Bilakovics J, Brown DA, Xu X and Nerenberg M. (1992). *Science,* **258,** 1792–1795.
Li Q, Lu Q, Hwang JY, Buscher D, Lee KF, Izpisua-Belmonte JC and Verma IM. (1999a). *Genes Dev.,* **13,** 1322–1328.

Li Q, Van-Antwerp D, Mercurio F, Lee KF and Verma IM. (1999b). *Science,* **284,** 321–325.
Li Q and Verma IM. (2002). *Nat. Rev. Immunol.,* **2,** 725–734.
Li XH, Fang X and Gaynor RB. (2001). *J. Biol. Chem.,* **276,** 4494–4500.
Li Y, Kang J, Friedman J, Tarassishin L, Ye J, Kovalenko A, Wallach D and Horwitz MS. (1999c). *Proc. Natl. Acad. Sci. USA,* **96,** 1042–1047.
Li ZW, Chu W, Hu Y, Delhase M, Deerinck T, Ellisman M, Johnson R and Karin M. (1999d). *J. Exp. Med.,* **189,** 1839–1845.
Lupas A, Van Dyke M and Stock J. (1991). *Science,* **252,** 1162–1164.
Makris C, Godfrey VL, Krahn-Senftleben G, Takahashi T, Roberts JL, Schwarz T, Feng L, Johnson RS and Karin M. (2000). *Mol. Cell,* **5,** 969–979.
Marriott SJ, Lemoine FJ and Jeang KT. (2002). *J. Biomed. Sci.,* **9,** 292–298.
May MJ, D'Acquisto F, Madge LA, Glockner J, Pober JS and Ghosh S. (2000). *Science,* **289,** 1550–1554.
Mercurio F, Murray BW, Shevchenko A, Bennett BL, Young DB, Li JW, Pascual G, Motiwala A, Zhu H, Mann M and Manning AM. (1999). *Mol. Cell. Biol.,* **19,** 1526–1538.
Mercurio F, Zhu H, Murray BW, Shevchenko A, Bennett BL, Li J, Young DB, Barbosa M, Mann M and Rao A. (1997). *Science,* **278,** 860–866.
Miller BS and Zandi E. (2001). *J. Biol. Chem.,* **276,** 36320–36326.
Mori N, Shirakawa F, Shimizu H, Murakami S, Oda S, Yamamoto K and Eto S. (1994). *Blood,* **84,** 2904–2911.
Nerenberg M, Hinrichs SH, Reynolds RK, Khoury G and Jay G. (1987). *Science,* **237,** 1324–1329.
Ng PW, Iha H, Iwanaga Y, Bittner M, Chen Y, Jiang Y, Gooden G, Trent JM, Meltzer P, Jeang KT and Zeichner SL. (2001). *Oncogene,* **27,** 4484–4496.
Orlowski RZ and Baldwin Jr AS. (2002). *Trends Mol. Med.,* **8,** 385–389.
Poyet JL, Srinivasula SM, Lin JH, Fernandes-Alnemri TF, Yamaoka S, Tasichlis PN and Alnemri ES. (2000). *J. Biol. Chem.,* **275,** 37966–37977.
Prajapati S and Gaynor RB. (2002). *J. Biol. Chem.,* **277,** 24331–24339.
Ranson M and Sliwkowski MX. (2002). *Oncology,* **63,** 17–24.
Robek MD and Ratner L. (1999). *J. Virol.,* **73,** 4856–4865.
Rothwarf DM and Karin M. (1999). *Sci. STKE,* **26,** RE1.
Rothwarf DM, Zandi E, Natoli G and Karin M. (1998). *Nature,* **395,** 297–300.
Rudolph D, Yeh WC, Wakeham A, Rudolph B, Nallainathan D, Potter J, Elia AJ and Mak TW. (2000). *Genes Dev.,* **14,** 854–862.
Scheidereit C. (1998). *Nature,* **395,** 225–226.
Schmidt-Supprian M, Bloch W, Courtois G, Addicks K, Israel A, Rajewsky K and Pasparakis M. (2000). *Mol. Cell,* **5,** 981–992.
Takeda K, Takeuchi O, Tsujimura T, Itami S, Dachi O, Kawai T, Sanjo H, Yoshikawa K, Terada N and Akira S. (1999). *Science,* **284,** 313–316.
Tanaka A, Takahashi C, Yamaoka S, Nosaka T, Maki M and Hatanaka M. (1990). *Proc. Natl. Acad. Sci. USA,* **87,** 1071–1075.
Tanaka M, Fuentes ME, Yamaguchi K, Durnin MH, Dalrymple SA, Hardy KL and Goeddel DV. (1999). *Immunity,* **10,** 421–429.
Tarassishin L and Horwitz MS. (2001). *Biochem. Biophys. Res. Commun.,* **285,** 555–560.
Tegethoff S, Behlke J and Scheidereit C. (2003). *Mol. Cell. Biol.,* **23,** 2029–2041.
Tsukahara T, Kannagi M, Ohashi T, Kato H, Arai M, Nunez G, Iwanaga Y, Yamamoto N, Ohtani K and Fujii M. (1999). *J. Virol.,* **73,** 7981–7987.
Whiteside ST and Israel A. (1997). *Semin. Cancer Biol.,* **8,** 75–82.
Xiao G, Harhaj EW and Sun SC. (2000). *J. Biol. Chem.,* **275,** 34060–34067.
Yamamoto Y and Gaynor RB. (2001). *J. Clin. Invest.,* **107,** 135–142.
Yamamoto Y, Kim DW, Kwak YT, Prajapati S, Verma U and Gaynor RB. (2001). *J. Biol. Chem.,* **276,** 36327–36336.
Yamaoka S, Courtois G, Bessia C, Whiteside ST, Weil R, Agou F, Kirk HE, Kay RJ and Israel A. (1998). *Cell,* **93,** 1231–1240.
Ye J, Xie X, Tarassishin L and Horwitz MS. (2000). *J. Biol. Chem.,* **275,** 9882–9889.
Yoshida M. (2001). *Annu. Rev. Immunol.,* **19,** 475–496.
Yoshida M, Miyoshi I and Hinuma Y. (1982). *Proc. Natl. Acad. Sci. USA,* **79,** 2031–2035.
Zandi E, Rothwarf DM, Delhase M, Hayakawa M and Karin M. (1997). *Cell,* **91,** 243–252.
Zhang SQ, Kovalenko A, Cantarella G and Wallach D. (2000). *Immunity,* **12,** 301–311.